Aircraft measurement of the probability distribution of precipitation rate and liquid water content in the hurricane

Robert A. Black[1]

[1]NOAA/OAR/AOML

Miami, FL

John Hallett[2]

[2]Desert Research Institute

Reno, NV

Abstract

Aircraft measurement of precipitation in the hurricane leads to insights into its origins, to interpretation of observed radar echo, to estimates of surface precipitation rates not measurable by other techniques and to design criteria for aircraft and surface instruments subject to a harsh environment. Analysis of data obtained by optical array sensors provide greater insight into these events when analyzed as a probability distribution function for data sets selected on a regional, hurricane location, or hurricane evolution basis. Liquid water content, precipitation rate and radar reflectivity are inferred from cross-sections of particle images. Each sequence, from seconds to seasons is presented in a probability format to display changing functional relationships for the selected intervals. The probability of intercepting a given quantity during a flight provides guidance in required instrument sensitivity together with the frequency of precipitation and liquid water content events for given rainfall totals.

1. Introduction

Measurements of precipitation rate and liquid water content (LWC) are conveniently made from aircraft using imaging instruments to provide sequential values along a flight path requiring averaging times of about 5 seconds for sufficient statistical reliability. At a true airspeed (TAS) of ~130 ms^{-1}, turbulent motions (a few percent of the mean wind speed) are negligible compared to the aircraft motion and have little effect on the airborne drop size distribution (DSD) measurements. The aircraft is also more efficient at collecting rain data, as the it can be flown directly into the rain. Precipitation measurement at the surface requires correction for wind speed, depends on the rain advecting over the gauge and often on wind direction because of terrain inhomogeneities and turbulence around the gauge. Because of these effects, aircraft measurement of rainfall is superior. This is subject to the assumption that the precipitation measured at altitude eventually reaches the surface, possibly affected by wind or fall speed sorting, clustering by particle size, as well as the collision-coalescence process (List et al., 1987).

The National Oceanic and Atmospheric Administration (NOAA) has been collecting airborne particle image data in tropical storms and hurricanes for > 30 years, sampling a wide variety of storm types, peak wind speeds, environmental conditions and altitudes. This work compiles some of this data in a manner amenable for comparison with model output, and produces rainfall statistics as a function of precipitation intensity. The characteristics of any meteorological system may be conveniently expressed as a probability of occurrence of the quantities of interest over a defined range of conditions in space or time. The fundamental question is the physical implication of the observed Probability Distribution Function (PDF hereafter) distributions. Each plot includes data from both stratiform and convective precipitation

within the same hurricane created by a combination of precipitation forming mechanisms which have similar causes, yet are completely unrelated to each other through a direct physical process. There is also an implication that within each set of data there could be a few large values not related to physical process at all but to a probability of random events, with all that implies.

Other researchers have presented related information using the PDF format to display other meteorological parameters. Chai and Hallett (1981) was the first instance we know of where a probability plot was used to show that surface snow precipitation events in the Sierra Nevada in California could be portrayed as the fraction of the total precipitation falling as a function of precipitation rate; within a season, snowfall could be characterized to show that most precipitation occurred near a specific rate and that the time spent at a given precipitation rate fell approximately exponentially with time. Such an event would be shown clearly with a properly constructed PDF. Zipser and LeMone (1980) used a probability plot with updraft measurements from the GATE (GARP Atlantic Tropical Experiment) to characterize the vertical motions. Tsinkidis and Georgakakos (1999) compared model rainfall PDF's with PDF's of rainfall derived from radar reflectivity data observed in the Western Pacific during the TOGA-COARE (Tropical Oceanic Global Atmosphere - Coupled Oceanic-Atmospheric Response Experiment) project to show the effect of various parameterization methods. Recently, Tapiador and Sanchez (2008) compared predictions of future European precipitation climatologies generated from an ensemble of models by comparing PDF's. Yuter and Houze (1995) showed that for Florida cumulonimbi, the probability of vertical velocity, radar reflectivity and differential reflectivity could be described by similar probability plots whose magnitude varied with height. For surface precipitation, Larsen et al. (2005) found that under 1 - 5-s averaging times, several 10-20 minute periods free of any drop clustering occurred in late winter and early spring precipitation events at

Wallops Island, Va., suggesting that a static equilibrium DSD List, (1988) occasionally occurs at these time scales. With such a DSD, integral parameters such as reflectivity, mass concentration, and number concentration are constant functions of the rain rate. A PDF of such rain, if it is common in tropical rain, should be noticeably different from non-tropical rain. Hallett and Rasmussen (2006) showed that high resolution snow precipitation events in Reno, NV for individual storms could similarly be portrayed, tending to a convergence when spectra from 3 similar storms were combined. Other equilibrium DSD's have been reported in tropical rain (Atlas and Ulbrich, 2000) resulting from the collision-coalescence process or updraft suspension of drops. Whether such equilibrium DSD's exist in the hurricane is not known, but higher temporal resolution particle size distributions than are presently available are needed to determine if either "raindrop clustering" or "equilibrium DSD's" occur.

In a hurricane environment, the probability of a given precipitation rate or a given volume or mass content of precipitation both contribute to the physical understanding of the system and its meteorological effects. The volume and mass content provides information on the ice accretion rate on any penetrating aircraft and magnitude of radar reflectivity whereas the precipitation rate, [affecting engine performance], is to be compared with events at the surface or with precipitation rates empirically derived from radar reflectivity. The overall probability of occurrence of these different quantities specify the upper limits of design desirable for surface precipitation and aircraft measurement instruments.

Different approaches are available for acquiring and displaying such data. Optical array instruments (such as the 2D-P imaging probe) where the projected drop image area is assumed to be symmetrical and provides particle size and number concentration from which the volume and fall velocity are derived are now the standard to which all others are compared. For ice or mixed

phase particles it is necessary to either measure or infer particle density (Gardner and Hallett 2009) independently to estimate mass, leading to a much greater uncertainty. For this reason, we limit our discussion to rainfall.

2. Data Set

a. Display protocol

Choosing data sets and display methods that are suitable for both model comparison and differentiation between changing climatic regimes requires a subtlety of approach. First, it is necessary to limit a regime from regional, time and process considerations. Here we concentrate on aircraft measurements of hurricane rainfall measured near 3 km MSL at temperatures near +12ºC under conditions of only slowly changing storm evolution. This is the altitude from which the vast bulk of the airborne drop size distributions were obtained. Different times within each flight in a storm may be chosen to avoid contamination of the DSDs by ice particles, as flight altitude varied somewhat. Data chosen for analysis are therefore from multiple times during a particular hurricane flight to give combined data as displayed in each plot; in principle such sets could be combined as a larger data base. In this data, the file naming convention is as follows: The first letter is the first letter of the storm name, followed by the flight date and a letter designating the WP-3D aircraft: H for NOAA-42, and I for NOAA-43. Hence, i810926I represents the 8'th named storm (Irene), on September 26, 1981, from NOAA-43. This study utilized the historical (1977-1992) hurricane rainfall data as the baseline for hurricane rainfall. New rainfall data obtained in 2005 and surface rainfall data obtained in Miami, Florida from 11 August – 10 November 2008 are compared with the historical data.

b. Measurement protocol

Drop diameters are measured and accumulated over an interval of 5-6 s (about 800 m of flight path) and a sample volume of 1 - 3 m^3, to be comparable with the length of the WP-3D lower fuselage radar range gate. Precipitation rate, liquid water content and radar reflectivity are calculated from the DSDs and displayed as a probability over the entire storm. An advantage of this approach is that similar predictions from a model storm can be formulated for comparison using identical probability plots. Independent drop size spectra are readily obtained along an aircraft flight path (which needs to be specified, Liu and Hallett 1998), to provide suitable numbers of drops per spectrum, ~200 drops for 32 size bins to provide adequate statistics (~10 ±3 drops per bin) for each individual measurement.

For the historical storms, DSD's were obtained with the Particle Measuring Systems (PMS) 2D-P optical array probe (Knollenberg, 1981). Newer versions of these probes (with faster electronics and an optical array with twice the number of photodiodes) manufactured by Droplet Measurement Technologies (DMT) were used in 2005. During penetrations of heavy rainfall, the old 2-D image probes were routinely overloaded and taking no data, thereby possibly undercounting the DSD most in the area where the particle concentrations were greatest. The new DMT probes obtain data much faster without overloading compared to the old probes, and they have better bean orifices for preventing splashes from entering the data stream. This in turn creates cleaner distributions, with less scatter and fewer large splash images, which can skew the old data's reflectivity and LWC calculations toward high values relative to the newer data. The DMT Precipitation Imaging Probe used in this study had a 6.4 mm array width at 0.1 mm diode

resolution. The particle image data were cleaned of artifacts and splashes using the methods presented in Black and Hallett (1986), and the size spectra were also accumulated for 5 or 6 seconds (~800 m along the flight path), depending on the year in which they were collected. Number concentrations as small as ~1 drop per cubic meter and as large as 300 l^{-1} within the probe size limits are detectable with these probes. As in Black and Hallett (1986), sizing was performed on the images using the "center in" technique, where the image center was defined as being the midpoint of the longest dimension parallel to the direction of flight, provided that the longest dimension was not on the edge of the array. Accepted image size for images whose largest dimension exceeded 0.8 mm was determined by fitting an ellipse to the image, computing the area of the ellipse, then computing the equivalent circle diameter by assuming that the ellipse area equaled the drop cross-section. Density functions of the parameters derived from the n-second average size distributions were computed and DSD's with number concentration < 0.001 L^{-1} excluded. Bin widths were chosen for readability such that most bins contained three or more samples.

Only in the case of the i810926I flight was substantial flight time spent in the strong convection and this is reflected in the higher radar reflectivities encountered. The other flights consisted of the more common "Figure 4" legs, with radial legs through the storm center separated by 60 – 90° in azimuth. The n840922I and n840924I flight tracks are shown in Marks et al. (1992) and are good examples of the standard flight pattern, which is intended to obtain the tangential wind envelope and Doppler wind analyses. In the case of the historical data, no effort was made to specifically limit penetrations of the high-reflectivity areas of the storm, whereas such areas are under represented in the newer (2005) data. The limits chosen to display the rain rate and Liquid Water Content (LWC) plots show the bulk of the data. Larger values of these

quantities occasionally exist, but these are few. In the case of the radar reflectivity, some computed values were less than zero (not plotted), but all are included in the probability density computation.

For comparison purposes, we also present rainfall measurements obtained on the roof of the AOML building in Miami, Florida from August 11 through November 10, 2008. These measurements were made using an experimental hot-plate raingauge (Figure 1). This device consists of two identical 13 cm diameter heated plates, one facing up and the other down and separated by a 7 mm thick insulator. The top plate measures the rain, the bottom plate measures the wind speed. Temperature is measured by a solar-shielded thermistor mounted on the 1 m support pole. Plate calibration was done by wetting each plate with water from a syringe at a known rate, which yielded an estimated maximum rain rate of 53 mm hr^{-1} at a wind speed of 50 ms^{-1}. At lower wind speeds, the maximum detectable rain rate increases. The absolute accuracy of the rain accumulation is within 10% and the precision is 0.1 mm. The minimum rain rate detectable is 0.4 mm hr^{-1}, more than 10 times larger than the minimum rain rates of ~ 0.01 mm hr^{-1} from the airborne probes. The gauge was mounted on the roof of the NOAA/AOML building in Miami, Florida at approximately 15 m from the ground from August 11 to Nov. 10, 2008. The AOML building is on the island of Virginia Key about 300 m from the shoreline and the prevailing winds are from the east to southeast off the sea. The gauge was strapped to a railing anchored to the building in order to withstand hurricane force winds; the strongest winds encountered this year were only ~ 20 ms^{-1}. Sources of error include the wind speed calibration, splashing and runoff when the rain accumulation exceeds the capacity of the heaters to evaporate it. These effects limit the observable rainrate to R < ~70 mm hr^{-1}. The rubber bands visible in the photo were installed 25 September 2008 to limit runoff, to be measured a little later.

c. Results

Plots are presented here from a variety of storms using exclusively rainfall data. Summary information about the storms chosen are presented in Table 1. Figure 2 shows the PDF and cumulative rain rate from four storms sampled in the late 1970s to early 1980s. These are representative of storms in which the higher maximum rain rates were sampled, with 90% cumulative probability (CP) rain rates between 28 to 80 mm h^{-1}. They are grouped by 90% CP rain rate (RR) to represent the typically heaviest rainfall encountered rather than an absolute maximum, but other criteria were considered. Figure 2A shows the PDF's from the storm in which the aircraft spent more time than usual in the high-reflectivity areas. This is reflected in the maximum RR observed of 355 mm h^{-1} for 2A, and a 90% CP level of 80 mm h^{-1}. In contrast, the storm sampled for 2B was one of only 3 Saffir-Simpson scale (SS) category 4 (Simpson and Riehl, 1981) storms in this data set, with a rain rate maximum of only 238 mm h^{-1} but a 90% CP level of 48 mm h^{-1}. The 90% CP level in the cumulative distribution was exceptionally high in 2A1 due to the time spent in the convection on that flight. This flight was extraordinary, in a category of its own in all measured parameters. In contrast, the 90% CP RR for 2C1 was only 38 mm h^{-1}, and for 2D1, 28 mm h^{-1}, less than half that of 3A1. The 2C1 and 2D1 90% CP levels were low because on that flight, the bulk of the time was spent mapping the stratiform precipitation outside the eyewall, but the eyewall rain rate maximum was still large, hence the extended tail. Further, these high rain rate distributions generally have more samples at all rates > 20 mm h^{-1} than those in Figures 3 and 4.

Intermediate RR storms, with maxima from 149 mm h^{-1} to 76 mm h^{-1} (90% CP of 10 – 22 mm h^{-1}) are shown in Figure 3. As in all flights except that in Fig. 3A, flight patterns during these missions were rotating "figure-4" patterns flown for optimized characterization of the wind and reflectivity fields rather than microphysical sampling. These plots were arranged in the same way as in Figure 2. The slopes of the cumulative probabilities of these flights are steeper than for those in Figure 2, but there were still significant spectra with rain rates > 20 mm h^{-1}. This fact is shown by the fact that these cumulative distributions have shallower slopes at RR > 20 mm h^{-1} than those from the other flights.

Finally, Figure 4 shows rain rates from two hurricanes sampled in 2005. Figure 4A and 4B were at Category 1 on the SS scale, and the other two (4C and 4D) occurred when these storms were much stronger. Unlike the old data, during the 2005 season, the highest rain rate areas in the eyewall were avoided. These data were collected using the newer, much faster DMT probes that did not saturate, or overload when the rain rates got high, so the measurements from them are more reliable. Maximum RR values were generally lower than those in Figs. 2 and 3, ranging from 82 – 142 mm h^{-1}, and the 90% CP's are likewise smaller than those shown earlier. Qualitatively, the RR distributions are quite similar to those of the low RR storms in Fig. 3, even though the maximum rates are lower than those from Fig. 3, and the spread is less also. This shows that the prevalence of light rain (RR < 20 mm h^{-1}) in a hurricane is probably partly real, in accordance with Marks (1985) and Marks and Houze (1987), and not entirely an artifact of the sampling. Since the old probes spent considerable time in an "overload" condition at high rain rate, when the probe recorded no data, it will be interesting to use the newer probes in a high rain rate area for comparison.

A PDF of rainfall rate measurements made with an experimental hot-plate rainguage is shown in Figure 5. Notice the wider scale in the vertical axis (5A). This occurred because the raingauge does not measure rain rate less than 0.4 mm hr^{-1}, whereas the airborne probes do. When the PDF of RR computed from the airborne DSD's was derived for RR > 0.4 mm hr^{-1}, the vertical scale of those data were similar. These data reveal that 90% of all surface rain rate (Fig. 5B) in normal summer thunderstorms at this location is < 15 mm hr^{-1} and distributed similarly to that for the low RR and recent hurricanes (Figs. 3 and 4). This is evidence that for most S. Florida storms, the rainfall measured aloft in hurricanes is not significantly different from summer convective rainfall measured at the surface. This result is perhaps not so surprising, since both the surface rain at the AOML building and low RR hurricane rain is generated by modest (non-severe) convection in a relatively clean moist tropical oceanic air mass. However, there are some heavy rain periods in these data. Figure 6 shows one of the longest continuous heavy accumulation periods in the data set. It is seen that the bulk of the rain accumulation in any convective rain shower occurs during the brief periods when the rain rates are higher than about 25 mm hr^{-1}. Such rain rates are common in the summer S. Florida convective rainfall, and also in the hurricane eyewall.

Liquid water content is another parameter computed from the DSD's. The shape of the distribution of these values at small LWC does not change much with the storm, only the large end tails of the PDF's, where the one storm with stronger convection sampled more frequently has values that regularly exceed 2 g m^{-3}. This is shown clearly by Figs. 7-9, presented in the same order as the RR plots. The storms containing the larger samples of strong convective rain (Fig. 7) all have large end tails that extend to (and in some cases beyond) the extreme right of the scale, whereas for the storms without such samples, the cumulative LWC probability reaches

~100% at ~5 g m^{-3}, well below the adiabatic value of ~20 g m^{-3} obtained from lifting a parcel from a cloud base temperature at 25ºC. This has been noted before with hurricane convection (e.g. Ackerman 1963, Black et al. 1994) but not in conjunction with PDF's of optical array probe data. Again, the recent data (Figure 9) had cumulative distributions almost identical to those of Figure 7, with no LWC measurement exceeding 6 g m^{-3} and a 90% CP at ~1 g m^{-3}.

The PDF of radar reflectivity computed from the DSD's are presented in Fig. 10-12. Data were truncated at 0 dBZ, therefore some of the cumulative distributions do not sum to 100%. The storms with the highest reflectivities sampled are shown in Fig. 10. Again, the order of occurrence is the same as on the earlier plots. The peaks of the reflectivity distributions shown in Figs. 10A and 10C are skewed toward higher reflectivity, with a long tail of low reflectivity, unlike the other storms presented in Fig. 11, whose distributions are more symmetric about the peak than the others. Note the gradual buildup of the cumulative probability on the low end of Fig. 10A1 and 10C1 until reaching the 90% CP levels at 50 – 60 DBZ. Slightly smaller 90% CP's are found in the PDF's of the storms in 10B1 and 10D1. These storms were all relatively well developed but asymmetric, with ~75% of the eye containing most of the convection, surrounded by a large area of stratiform rain, whereas the storm sampled in Fig. 10B was more symmetrical. Such storms tend to have higer winds and a larger SS category.

PDF's like these are typical of old storm data sets, but this has little or nothing to do with the overall strength of the wind field. Fig. 12 shows the reflectivitiy PDF's from the four recent storms. Two of these storms (Fig. 12C and 12D) were major category 4 storms at the time of sampling. These data show much lower reflectivities and steeper cumulative distributions than the other hurricanes, even though they were sampled using modern probes that responded

without overloading. The median cumulative probabilities are around 40 dBZ in Fig. 10, 30 dBZ in Fig, 11, and 25 dBZ in Fig. 12. The probability distributions for these storms are more concentrated near the peak, and the 90% CP are all ~40 dBZ. This is largely a product of the flight path, as stronger reflectivity areas were avoided, thereby shifting the distribution maxima toward low reflectivity.

The foregoing discussion illustrates the substantial effects of the choice in flight path with respect to reflectivity on the precipitation measurements. The storm with the heaviest precipitation (I810926I, Fig. 10A) was only an SS category 2 at the time of observation. The storm with the strongest winds and second heaviest rainfall (a770901h, Fig. 10B) was strengthening from SS category 2 to category 4 at the time of observation. Of the more recent data, two flights occurred during the category 4 period, one each in hurricanes Katrina and Rita of 2005, yet these data showed little evidence of high reflectivity. The weaker hurricanes sampled with the standard "rotating figure 4" flight pattern were similar, except that the peak DBZ was smaller and the falloff at high reflectivity was not as steep. On the low reflectivity side, more of the probability distribution was to the left of the x-axis minimum. The median level of these plots (30 - 40 dBZ) is directly comparable to the vertical average reflectivity observed in 15 hurricanes by Black et al., (1996). In that study, the average reflectivity well below the melting level from the WP-3D tail Doppler radar was 32 - 38 dBZ, depending on altitude. Two of the flights included in that study are also included here.

These plots are also compared with the PDF (Fig. 13) generated over the model domain at the 3 km level from the MM5 simulation of H. Bonnie (1998) presented by Rogers et al. (2007). This PDF is very similar in shape to the high reflectivity PDF (Fig. 10A) from Hurricane Irene (1981), although the observed case is not as sharply peaked near the median. The vertical

axis is different because of the vastly greater number of samples that entered the observational data, and this plot used 5 dB bins instead of the 1 dB bin widths of Figures 10-12. The median reflectivity in this case is 45 dBZ, higher than almost all of the observed cases, and is also more peaked around the median. This shows the high bias of the model, because unlike the other cases, the flight data in this case also has a high bias in that strong convection was specifically targeted for the flight in Irene (Fig. 10A).

Conclusions

There are competing effects occurring that to some extent may compensate for the different flight strategies and the technological advance of the newer probes. During the 1980s and 1990's, hurricane research flights routinely penetrated the high reflectivity cores in the eyewall. The practice (since 2000) of avoiding the more reflective areas skews the distributions toward low rain rate and reflectivity, and may lead to erroneous conclusions concerning the prevalence (or lack thereof) of heavy precipitation in the hurricane.

The plots included here show that the probability of hurricane rain rates > 20 mm/h is small, with an exponential decay probability at 0.05, with the notable exception of the i810926I flight. The probability of LWC > 5 g m^{-3} is similarly small, with an exponential decay probability from 0.05, even in the most convective storms. Reflectivity plots from storms sampled prior to 1992 have maxima in the range 30 - 40 dBZ with a spread of ±10 dBZ, in accordance with earlier work such as Black et al. (1996), where all of the high reflectivity and rain rate values are found in the eyewall. The 2005 data reflectivity maxima were weaker, about 25 – 30 dBZ, in spite of the fact that two of those storms were major SS category 4 storms when they were

sampled. This result was the product of the flight paths chosen such that heavy rainfall was avoided whenever possible. If the precipitation measured aloft gets to the surface (a certainty in the humid tropics), then that rain rate PDF measured aloft (perhaps with reduced small drop concentrations) should be similar to that measured at very low altitude under high winds and turbulence, a difficult and dangerous measurement to make, especially from an aircraft. This was shown to be approximately true by the similarity of the PDF for rainrate from the low RR storms and the coastal Miami, Florida surface rainfall.

Plots like these demonstrate that frequency distributions could be meaningful in characterizing likelihood of precipitation events. We have shown that the choice of flight patterns can and does affect the distributions, but their ultimate use falls into the following categories: in quantifying changing climatic regimes (such as a changing moisture climate), which would change the frequency of heavy precipitation; in quantifying the probability of specific hurricane precipitation characteristics e.g. extra convective, excessively stratiform, multiple eyewalls, etc. They might also be useful in assessing the optimum sensitivity of instruments for aircraft measurements: do we really need to account for extremely heavy rainfall, or will devices that work at lower rain rate be adequate? Another question is how much precipitation ingestion is likely, and can a particular engine accommodate that rainfall without stalling?

Comparisons with the normal summer coastal rainfall in Miami, Florida revealed that the PDF of ordinary convective rainfall is very similar to the PDF of hurricane rain, even though the Miami data contained one (non-hurricane) torrential rain event. Heavy rainfall (RR > 50 mm hr^{-1}) is common in summer Florida convection, but it usually lasts only a few minutes. The difference in this instance is that during the torrential event, the heavy rain lasted for almost

an hour, and there were several heavy rain events that day leading to a 24 hr accumulation > 16 cm. In the hurricane, the heaviest rain is usually found in the eyewall, but that heavy rain does not normally linger over one spot on the surface. When it does, accumulations of several cm occur, defining a torrential rain event. Such events are of primary importance to emergency managers and first responders because of the flash floods that often accompany torrential rainfall. These images can also be directly compared with numerical model output PDFs. A PDF is one of the few means possible to directly compare model precipitation with actual measurements. These PDFs therefore may help to guide model design to finally make more accurate precipitation forecasts.

References

Ackerman, B., 1963: Some Observations of water content in hurricanes. *J. Atmos. Sci.*, **20**, 288 – 298.

Atlas, D. and C. W. Ulbrich, 2000: An observationally based conceptual model of warm oceanic convective rain in the tropics. *J. Appl. Meteor.*, **39**, 2165 - 2181

Black, M. L., R. W. Burpee, and F. D. Marks, Jr, 1994: Vertical motion characteristics of tropical cyclones determined with airborne Doppler radial velocities. *J. Atmos. Sci.*, **53**, 1887-1909.

Black, R. A. and J. Hallett, 1986: Observations of the distribution of ice in hurricanes. *J. Atmos. Sci.*, **43**, 802-822.

_____, and J. Hallett, 1999: Electrification of the hurricane. *J. Atmos. Sci.*, **56**, 2004-2028.

Chai J.and J.Hallett, 1981 An analysis of precipitation rate frequency for some Sierra Nevada storms. AMS Fourth Conference on Hydrometeorology, pp. j16-J26, Reno, NV.

Garner and Hallett, 2009: On the density of ice particles. (in review)

Hallett, J, and R. Rasmussen 2006, Characterization of Changing Precipitation Regimes, Paper 4.9, AMS 18'th Conference Climate Variability and Change, Atlanta, GA,

Knollenberg, R. G., 1981: Techniques for probing cloud microstructure. *Clouds, Their Optical Properties and Effects.* P. V. Hobbs and A. Deepak, Eds., Academic Press, 15-89.

Larsen, M. L, A. B. Kostinski and A. Tokay, 2005: Observations and analysis of uncorrelated rain. *J. Atmos. Sci.*, **62** 4071 – 4083.

List, R., N. R. Donaldson, and R. E. Stewart, 1987: Temporal evolution of drop spectra to collisional equilibrium in steady and pulsating rain. *J. Atmos. Sci.*, 44, 362-372.

Liu Y. and Hallett, J., 1998: On Size Distributions of Cloud Droplets Growing by Condensation: A New Conceptual Model. *J. Atmos. Sci.*, **55**, 527 –536

Marks, F. D., Jr., 1985: Evolution of the structure of precipitation in Hurricane Allen (1980). *Mon. Wea. Rev.*, **113**, 909 - 930.

Marks, F. D., Jr., and R. A. Houze, 1987: Inner core structure of Hurricane Alicia from airborne Doppler radar observations. *J Atmos. Sci.*, *44*, 1296-1317.

Marks, F. D., Jr., R. A. Houze, Jr., and J. F. Gamache, 1992: Dual-aircraft investigation of the inner core of Hurricane Norbert. Part 1: Kinematic Structure. J. Atmos. Sci., **49**, 919 – 942.

Rogers, R. F., M. L. Black, S. S. Chen, and R. A. Black, 2007: An evaluation of microphysics fields from mesoscale model simulations of tropical cyclones. Part 1: Comparisons with observations. *J. Atmos. Sci.* , **64**, 1811 - 1834

Simpson R. H., and H. Riehl, 1981: *The Hurricane and its Impact*, Louisiana State University Press, pp. 366-368.

Tapiador, F. J., and E. Sanchez, 2008: Changes in the European precipitation climatologies as derived by an ensemble of regional models. *J. Climate*, **21**, 2540 - 2557

Tsinkidis, D, and K. P. Georgakakos, 1999: Microphysical and large-scale dependencies of temporal rainfall variability over a tropical ocean. *J. Atmos. Sci*., **56**, 724 - 748.

Yuter, S. and R. A. Houze, Jr., 1995b: Three-dimensional kinematic and microphysical evolution of Florida cumulonimbus. Part II: Frequency distributions of vertical velocity, reflectivity, and differential reflectivity. *Mon. Wea. Rev.*, **123,** 1941–1963.

Acknowledgments

Too many people contributed to the collection of these data to be explicitly named, including but not limited to numerous personnel of the NOAA Aircraft Operations Center and the NOAA Hurricane Research program. We especially would like to acknowledge the help with the IDL software development provided by Dr. George Soukup of NOAA/AOML and ITTVIS Inc. John Hallett was supported in part by NSF contracts ATM0313581 and ATM 0722438.

Figure Captions

Figure 1 The DRI experimental hot-plate raingauge.

Figure 2 Higher reflectivity old data set. Note the preponderance of RR < 10 mm h^{-1}.

Figure 3: Low reflectivity old data set.

Figure 4: Recent storms RR distribution.

Figure 5: Surface rain rate PDF from coastal Miami, Florida, August 10 – November 11 2008.

Figure 6: Time history of the rainfall during the one torrential rainfall event on October 4, 2008.

Figure 7: High reflectivity storms LWC.

Figure 8: Low reflectivity LWC distribution.

Figure 9: Recent storms LWC distribution.

Figure 10: Reflectivity distribution, old high DBZ data.

Figure 11: Reflectivity distribution, low DBZ old data.

Figure 12: Reflectivity distribution, recent storms.

Figure 13: Reflectivity distribution from MM5 simulation of Hurricane Bonnie (1998).

Flight	Storm Category	Max Rain Rate (mm/h)	Max LWC (g m^{-3})	Max Reflectivity (dBZ)	Storm Name
a770901h	4	238	9.7	59	Anita
d790904h	2	76.1	3.1	50	David
i810926l	2	355	14.6	62	Irene
a830917h	1	149	5.6	54	Alicia
a830917i	1	126	5.3	54	Alicia
n840922i	3	464	18	62.8	Norbert
n840924i	2	249	10.3	55.6	Norbert
g900828i	2	162	8.2	54.9	Gustav
		NEWER	DATA		
K050825i	1	142.5	5.8	49.2	Katrina
K050828i	4	129.3	5.4	47.2	Katrina
R050920l	1	82.2	3.6	48	Rita
R050921l	4	111.5	4.9	51.2	Rita

Table 1: General characteristics of the included storms.

Figures

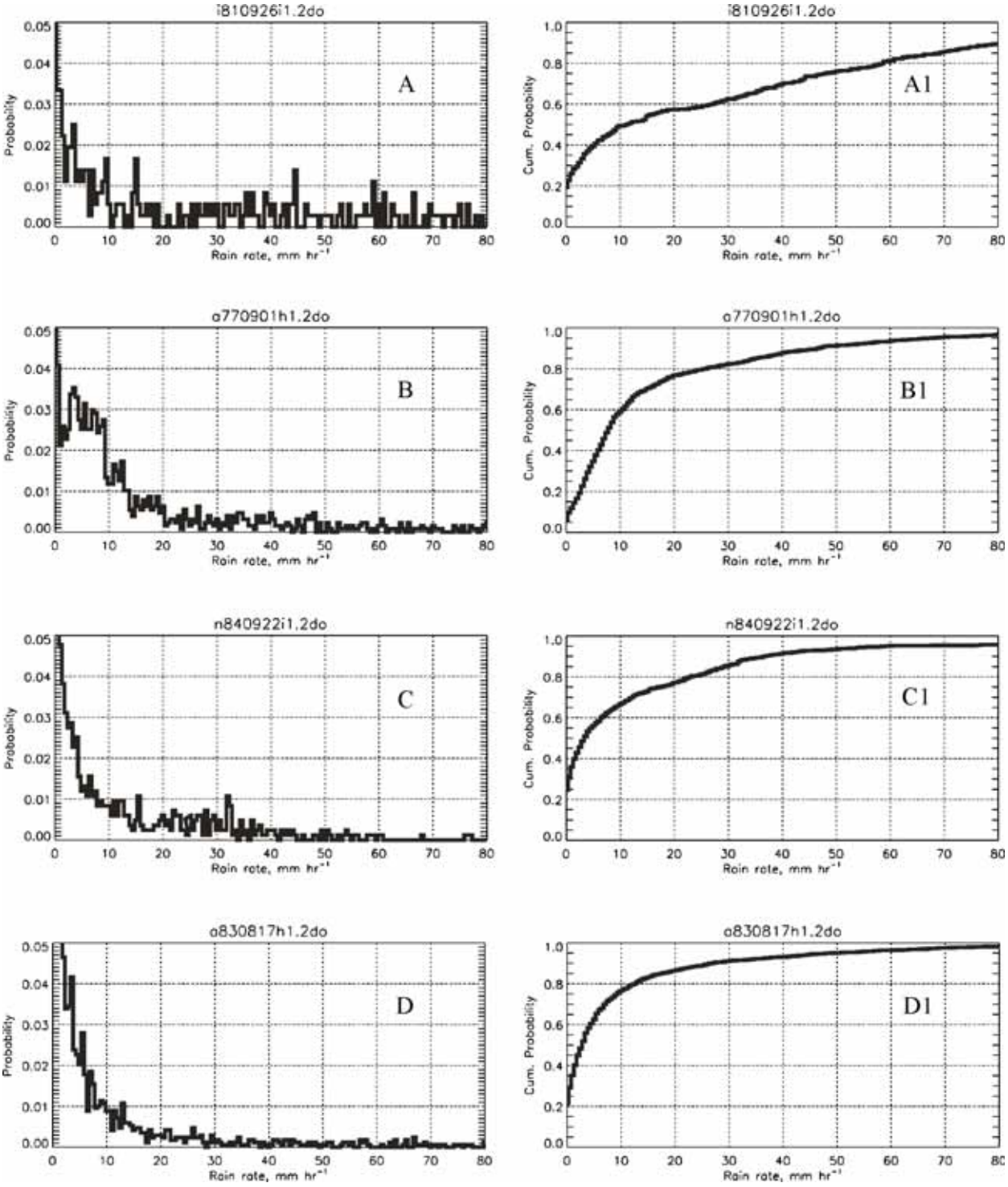

Figure 2. Higher reflectivity old (1977-1992) data set. Note the preponderance of RR < 10 mm h^{-1}.

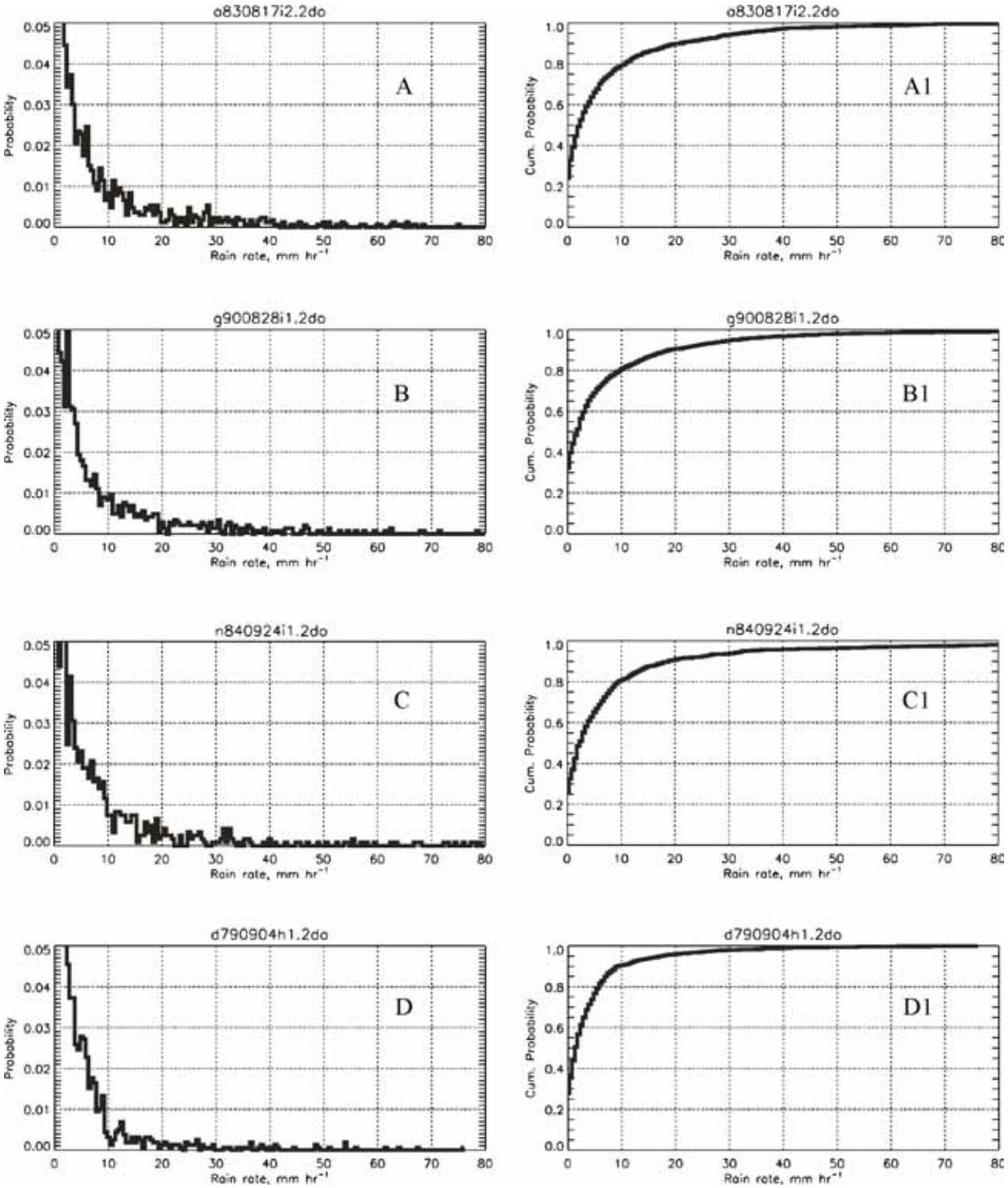

Figure 3: Low reflectivity old data set.

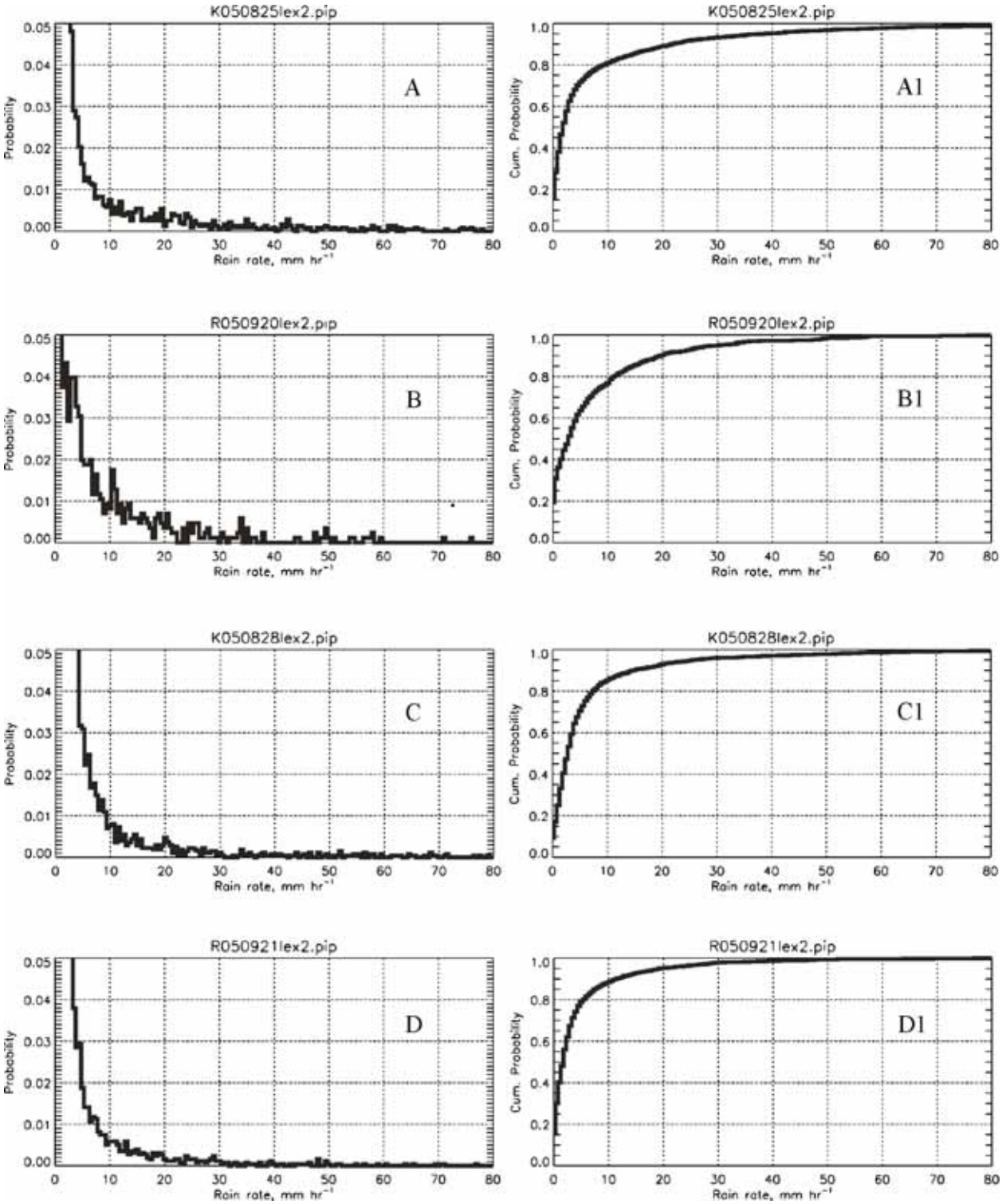

Figure 4: Recent storms RR distribution.

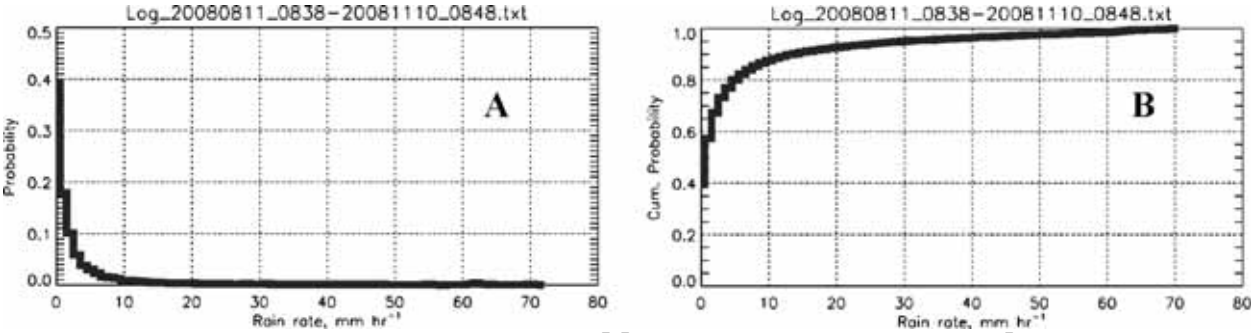

Figure 5: PDF of surface rainfall rate from Miami, Florida August 11 – November 10, 2008.

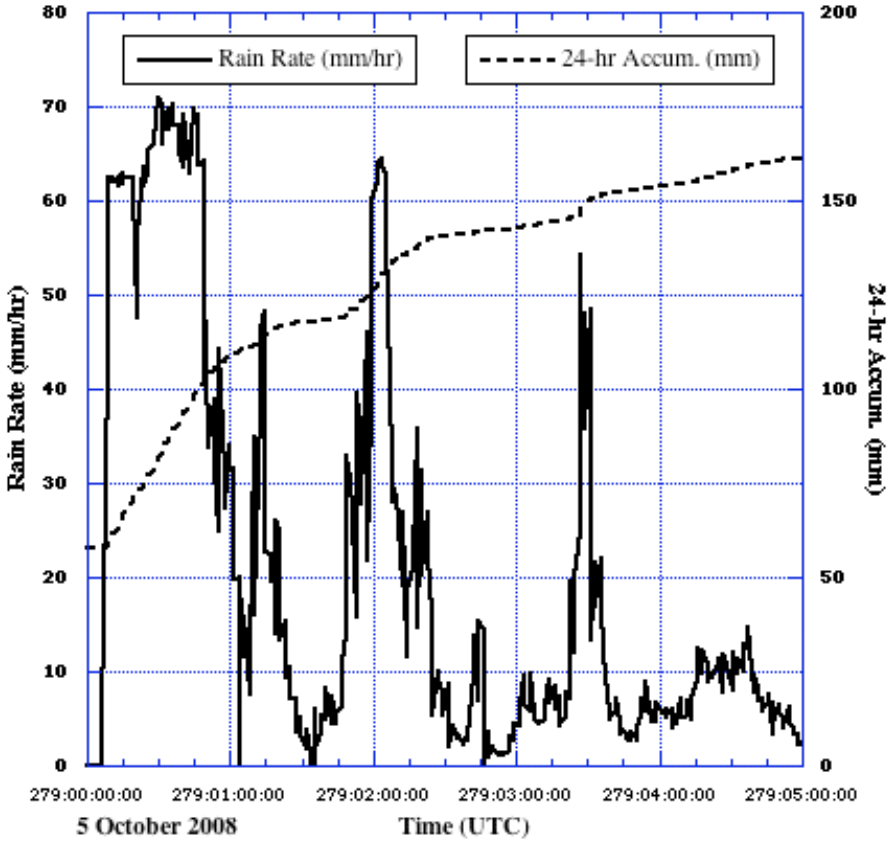

Figure 6. Rain rate and rain accumulation for the heaviest rain event of the period. Note that the steepest increases in the accumulation occur during the relatively short periods when RR > 50 mm hr^{-1}.

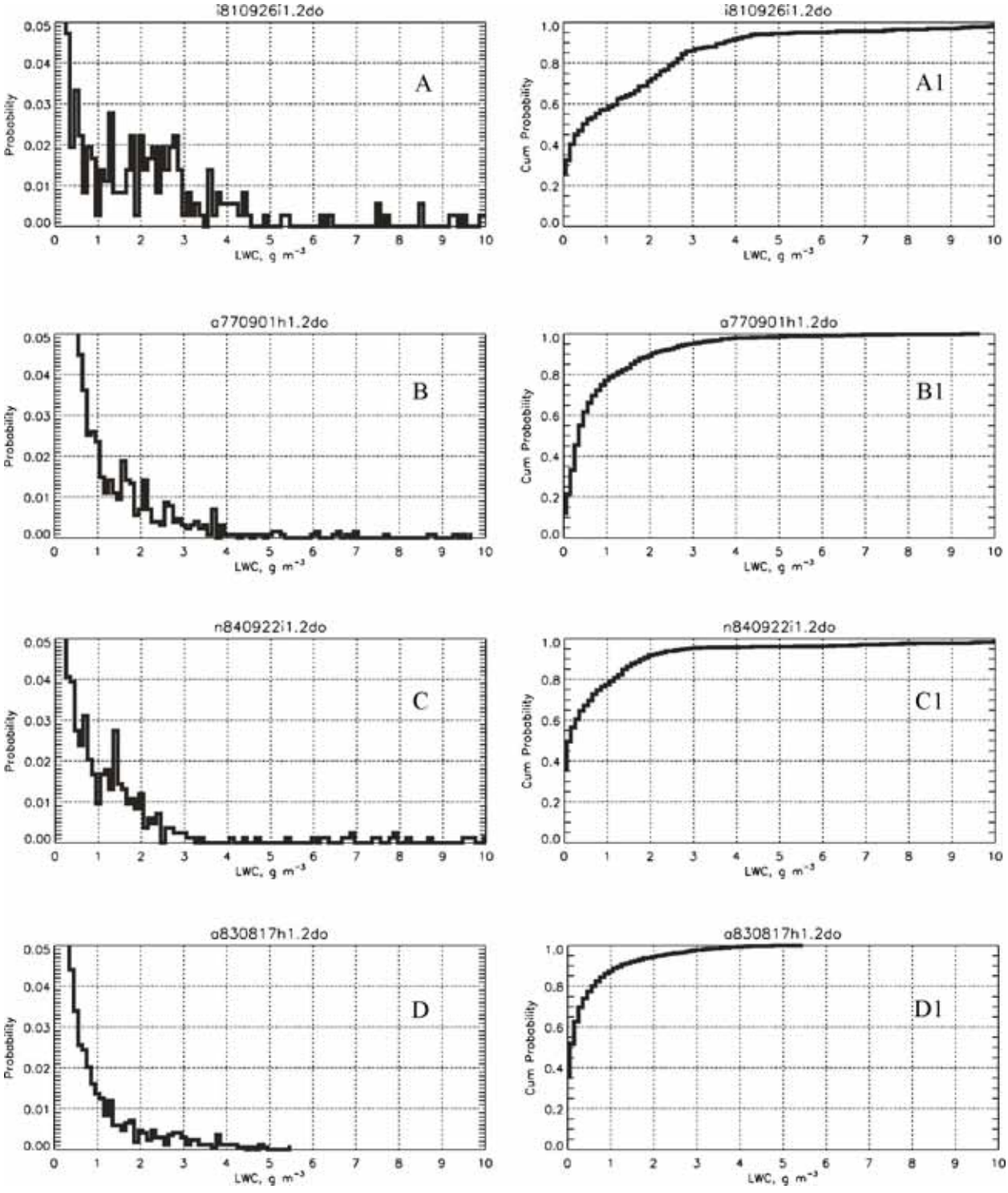

Figure 7: High reflectivity storms LWC.

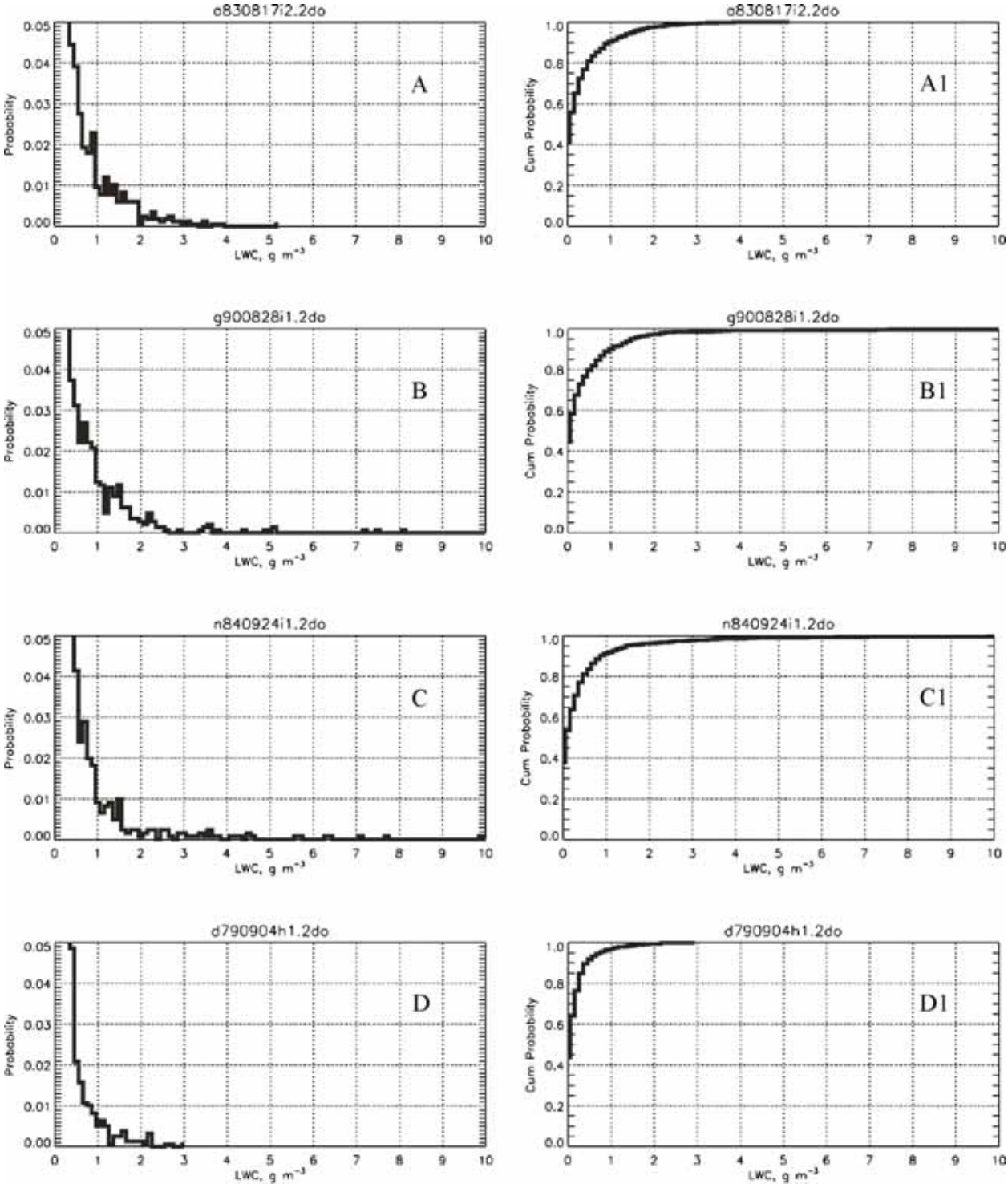

Figure 8: Low reflectivity LWC distribution.

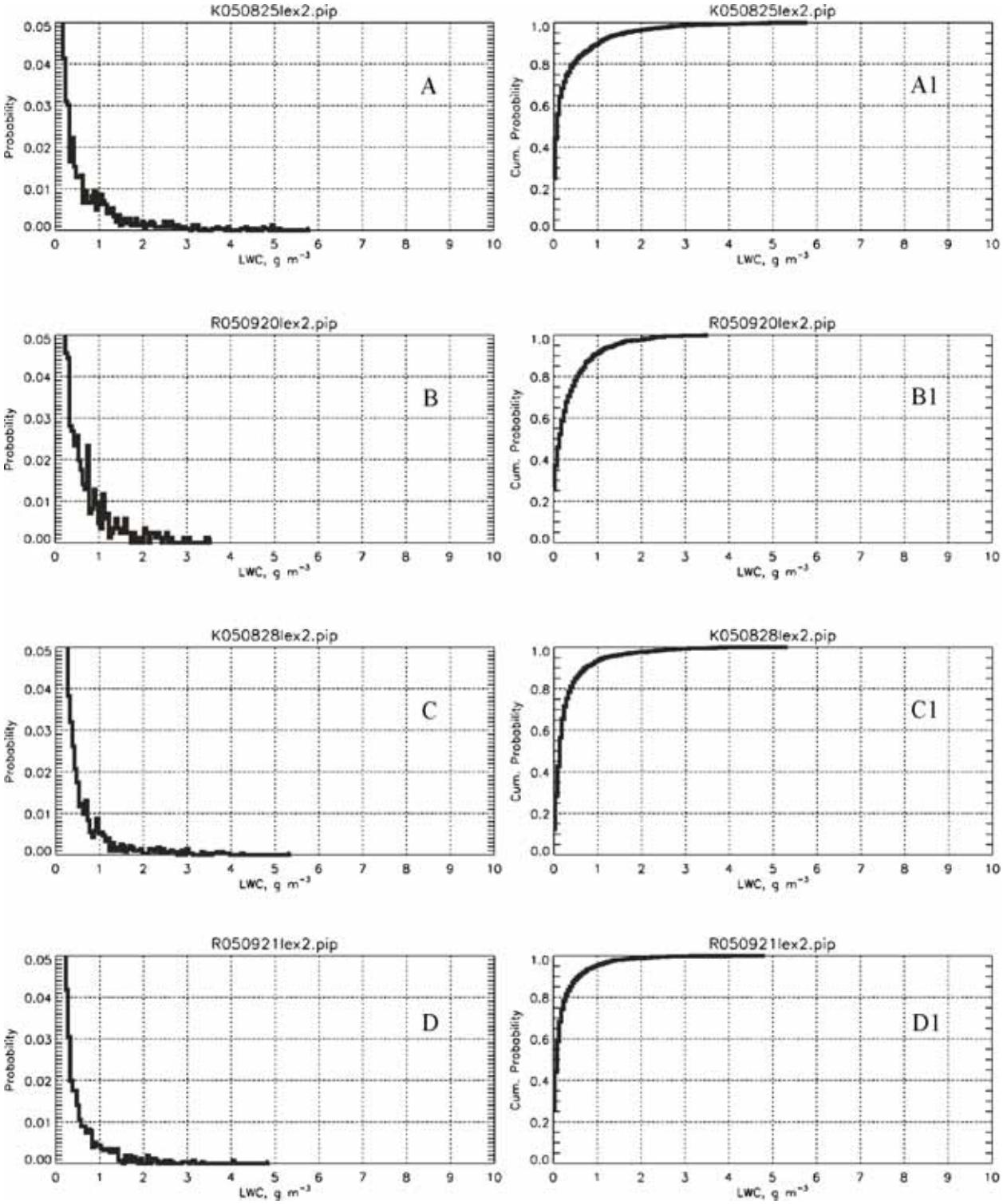

Figure 9: Recent storms LWC distribution.

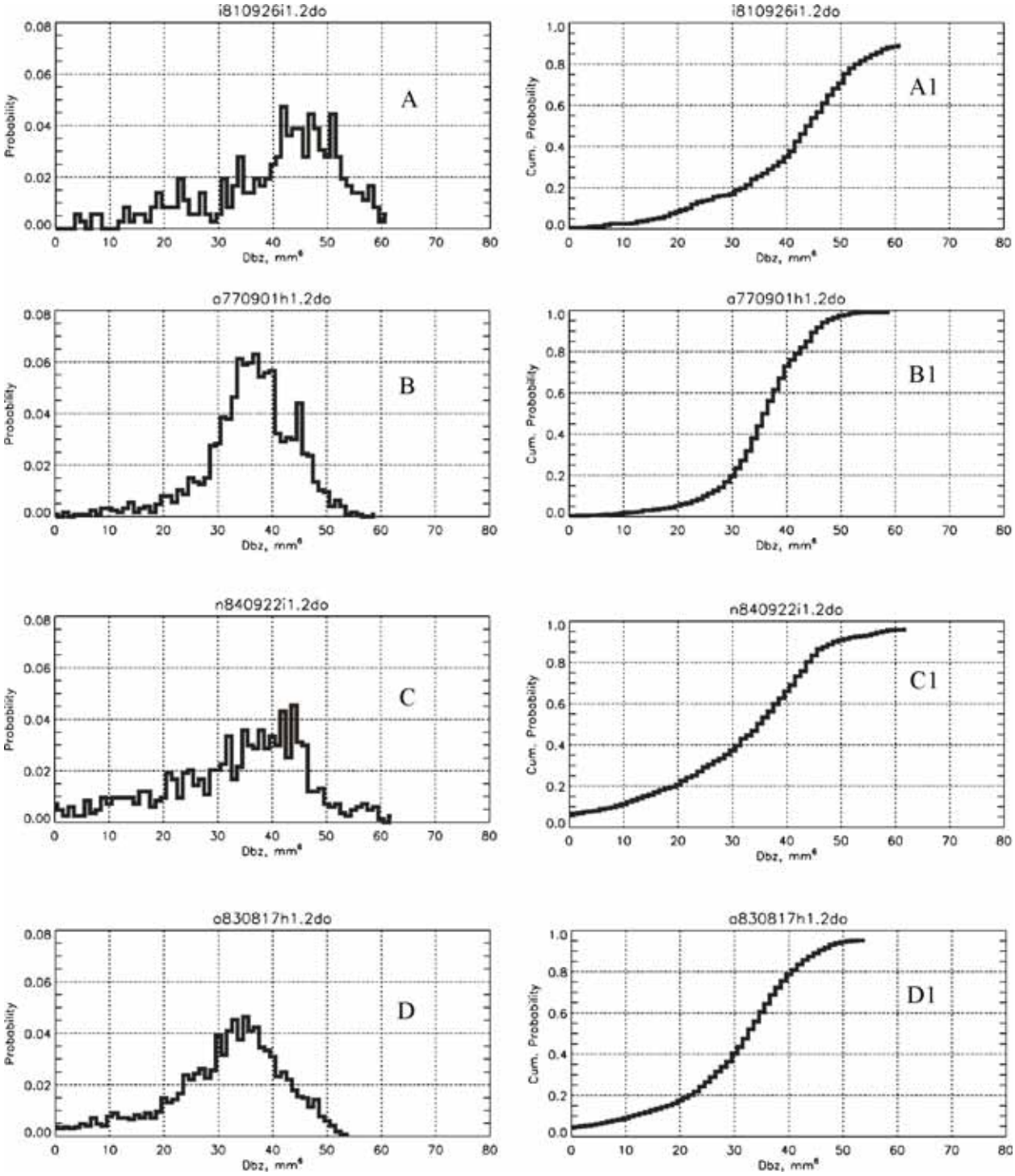

Figure 10: Reflectivity distribution, old high DBZ data.

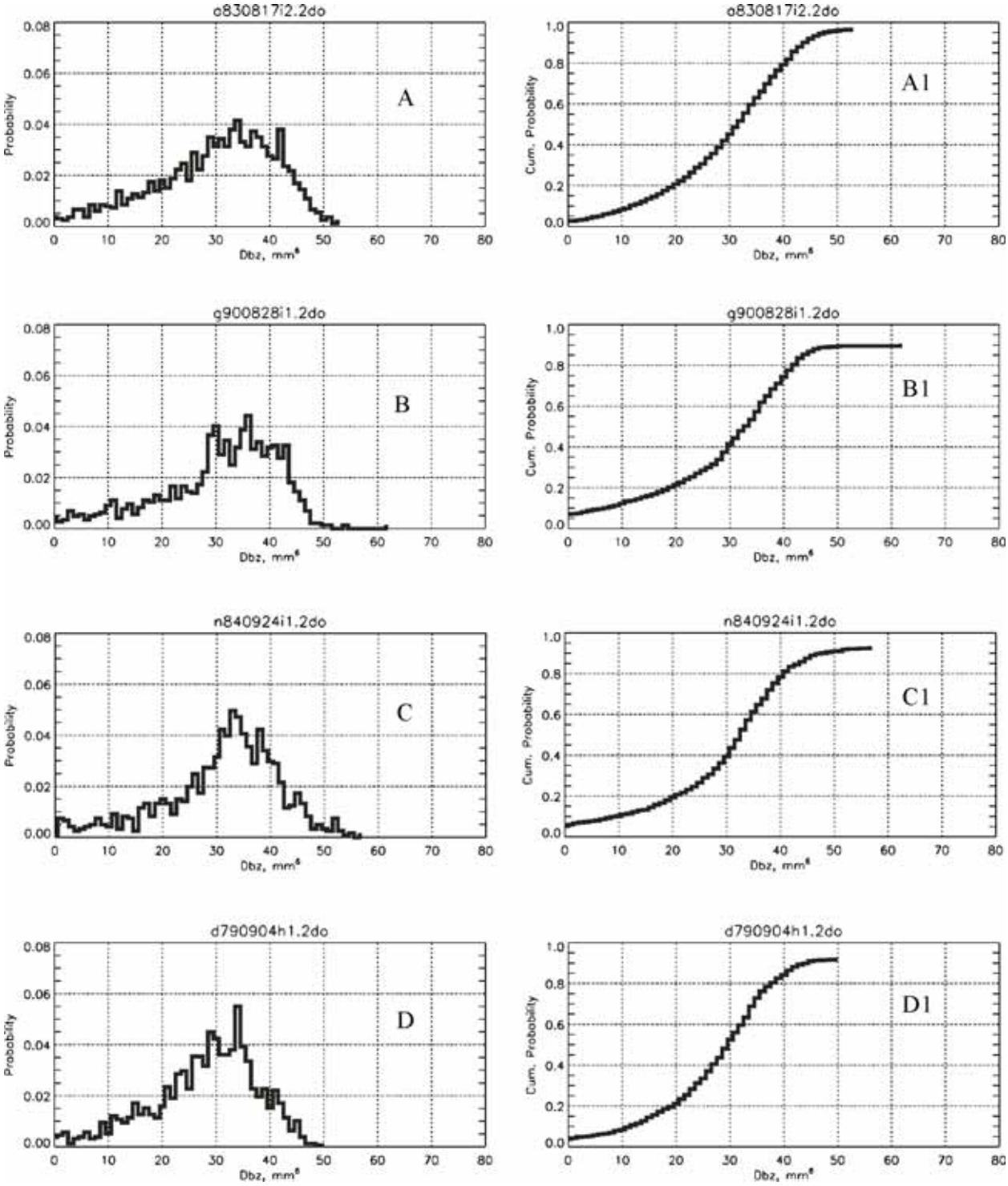

Figure 11: Reflectivity distribution, low DBZ old data.

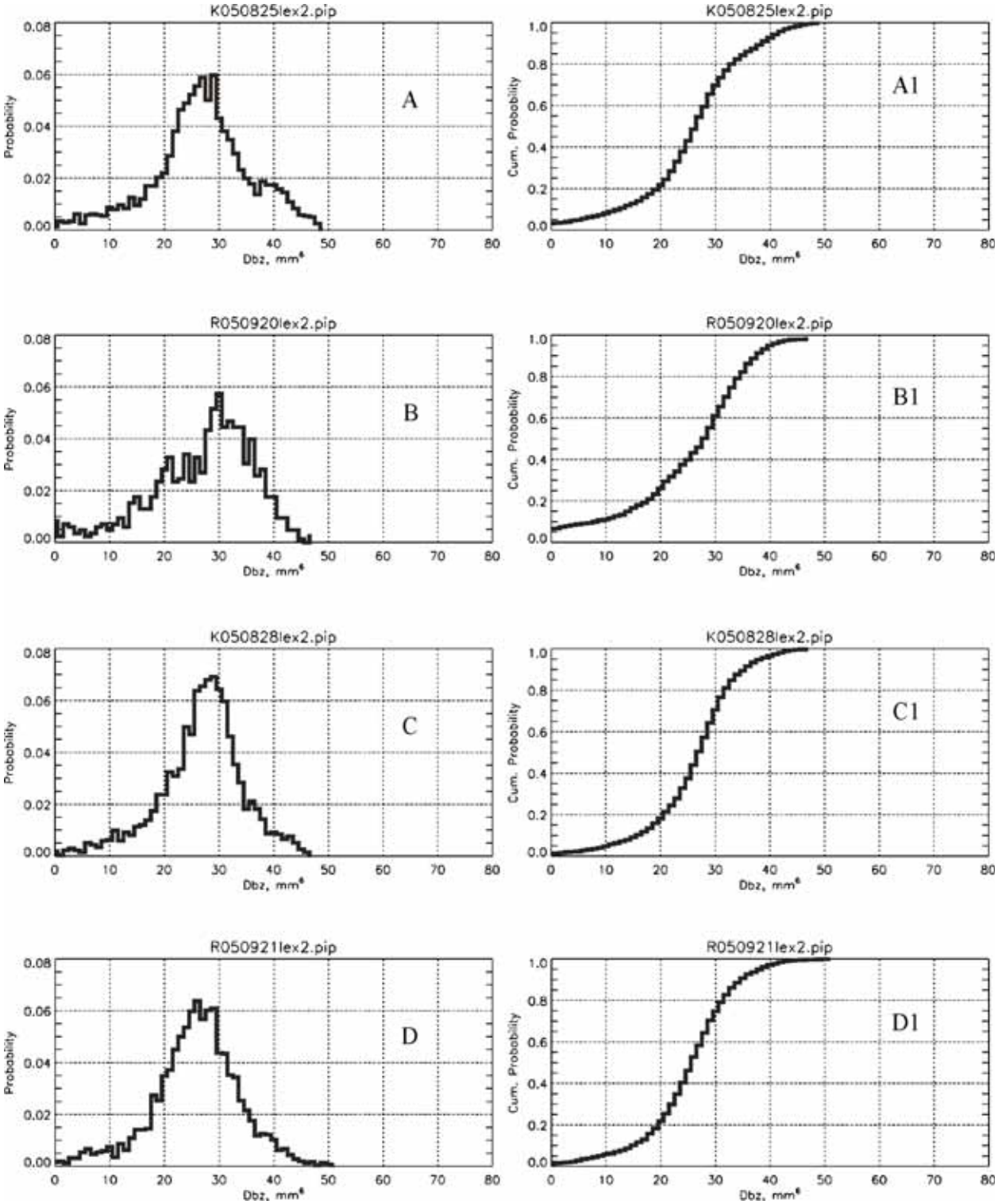

Figure 12: Reflectivity distribution, recent storms.

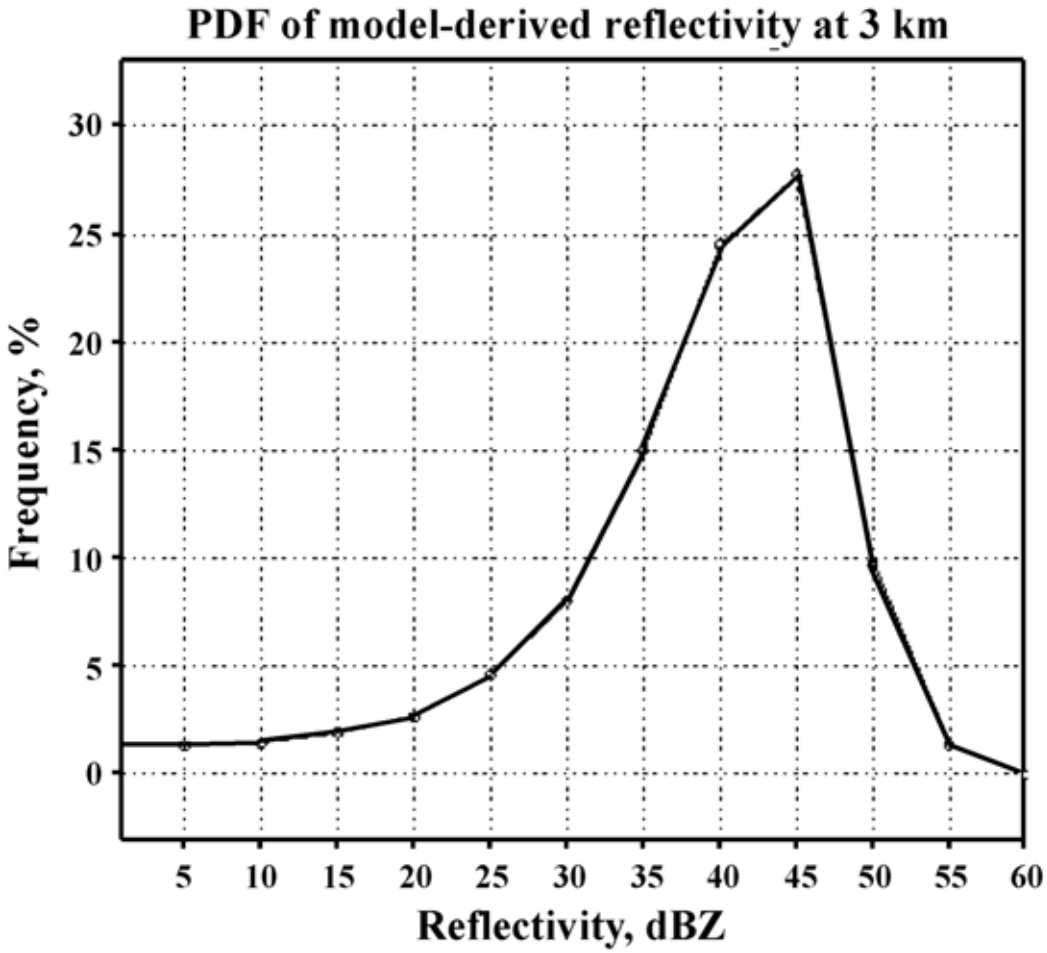

Figure 13: Reflectivity distribution from MM5 simulation of Hurricane Bonnie (1998).